

Dynamic and static strain aging in a high-manganese steel

Authors: *S. Wesselmecking, W. Song, W. Bleck*

Keywords: *Strain aging, high-manganese steel, C-Mn ordering, small angle neutron scattering, deformation behavior*

Abstract

Carbon containing high-manganese steels are susceptible to strain aging, which influences the mechanical properties during and after deformation. To understand the strain aging behavior of austenitic Fe-22Mn-1.3Al-0.3C high-manganese steel, dynamic as well as static strain aging were examined. Dynamic strain aging, occurring during deformation, was quantified by tensile tests at different strain rates. The strain localization during straining, was analyzed by digital image correlation. A decrease of strain rate increased the tensile strength and influenced the onset of a serrated flow. Static strain aging was quantified by interrupted tensile tests, combined with digital image correlation and small angle neutron scattering. The yield strength was increased due to static strain aging at room temperature within the period of days. The samples showed extended yield point (yield point elongation) and the effect was strengthened at higher pre-deformation. With small angle neutron scattering evidence of C-Mn ordering during aging was obtained and correlated.

Introduction

Austenitic high-manganese steels show outstanding properties, like high strain hardening, high energy absorption and high ductility ^{[1][2][3]}. Therefore, high-manganese steels are promising as next-generation structural materials in automotive and aerospace industries ^{[4][5][6][7]}. The high ductility is in particular based on their deformation mechanisms: transformation induced plasticity (TRIP) and twinning induced plasticity (TWIP) ^[8]. TWIP results in a superior combination of strength and ductility depending on stacking fault energy, grain size and chemical composition of the austenite phase ^{[9][10][11][1]}. Time dependent effects are less in focus of investigations but are known to have a strong influence on the deformation - like strain aging ^{[12][13]}. The conditions for strain aging are often interstitial elements, as carbon, interacting with dislocations or point defects ^{[14][15][16][17]}. Strain aging has to be distinguished between dynamic strain aging and static strain aging ^{[18][19]}.

Static strain aging appears after deformation and is influenced by the aging time and the applied deformation ^{[20][21][22]}. In ferritic steels it is used specifically to increase the yield strength of sheet material by a heat treatment integrated in paint lines. This so called bake hardening utilizes the Cottrell effect and requires a previously applied small deformation and a temperature that allows diffusive processes of the interstitially dissolved carbon ^[23]

[24]. The Cottrell effect is a long-range diffusion-controlled mechanism. In contrast to ferritic bcc structures, the diffusion rate in austenitic fcc is 10 to 100 times lower [25][26][27]. In addition, even if carbon atoms are in the vicinity of dislocations, the isotropic stress field of the carbon atoms in octahedral sites is much smaller in fcc than in bcc, reducing the possible pinning-effect of dislocations, making the effect negotiable [28].

A carbon-manganese ordering (C-Mn ordering) phenomena is reported to be responsible for strain aging in austenitic high-manganese steels [29][30][12]. Deformation in fcc steels comes along with shear on (111) planes, which is described to initiate a C-Mn ordering process [12][31]. Thereby, the carbon atom is displaced from an octahedral interstitial site into an energetically less favorable tetrahedral interstitial site in the crystal lattice [12]. The low activation energy, which is necessary for repositioning, increases the probability for a jump from a tetrahedral interstitial site into an octahedral site even at RT. This repositioning of carbon is expected into the energetically most favorable position, which is octahedral interstitial site, surrounded by as many manganese atoms as possible [32][33][12]. This C-Mn ordering evokes three important changes: 1.) an energetic minimization and thus a locally thermodynamically more stable system which promotes planar slip [34], 2.) locally enriched carbon and manganese contents and consequently local changes of SFE [35] and 3.) a proportionally stronger pinning of trailing partials increasing twinning [36].

Understanding the processes that take place during strain ageing and knowledge on the interaction of C-Mn ordering are important to control the mechanical properties and to facilitate industrial applicability [5]. Nevertheless, so far it is not possible to establish a clear connection between the formation of C-Mn ordering and the strain aging-related change in mechanical properties. In addition, while publications describe the influence of pre-deformation on the formation of a short-range order, the influence of rapid aging at room temperature is neglected. In order to obtain a comprehensive description, we investigate static and dynamic strain aging on one material. By using digital image correlation, we quantify and describe the aging-controlled, inhomogeneous deformation behavior during dynamic strain aging (serrated flow) and during static strain aging (pronounced yielding). In order to determine the correlation between an increase in stress, a change in deformation behavior and short-range ordering, we investigate precisely the change in the mechanical properties, the forming behavior and the formation of short-range structures by small angle neutron scattering.

Experimental

To describe the kinetics of static and dynamic strain aging in a high-manganese steel, we investigated the Fe-22Mn-1.3Al-0.3C alloy. Tensile tests were conducted and strain localization during testing was examined by digital image correlation. The kinetics of static strain aging were analyzed by correlating results from interrupted tensile tests with results from small angle neutron scattering (SANS).

The high-manganese steel with the chemical composition as listed in **Table 1** was vacuum-melted and ingot casted. The ingot material with the dimensions of 140x140 mm²

was forged to the dimension of 120x160 mm² at 1150 °C. Subsequently a homogenization heat treatment was performed at 1180 °C for 4 h. The homogenized ingot was hot-rolled at 1150 °C to a plate thickness of 3 mm in several passes. Cold-rolling to 1.5 mm was performed and the sheets were recrystallized at 700 °C for 60 min in a salt bath with an inhibitor to avoid nitrogenization. The recrystallized material had an average grain size of 5.3 µm.

Table 1 Chemical composition of the investigated TWIP steel Fe-22Mn-1.3Al-0.3C in wt.-%.

C	Mn	Si	P	S	Cr	Al	Fe
0.33	21.9	0.05	0.010	0.003	0.03	1.30	balance

Sub-size tensile specimens with an initial gauge length of 25 mm according to DIN EN ISO 6892 were extracted by water cutting transverse to rolling direction. A Zwick sample preparation machine was used to grind the edges and precisely adjust the parallel width. For the tensile tests a Zwick Z250 universal tensile testing machine was used. The parallel length of the samples was coated with acryl-based spray paint (white on black) to measure the strain by digital image correlation. It was used to describe the inhomogeneous deformation behavior occurring during plastic deformation and specially to characterize the local deformation during yielding. A GOM Aramis (Gom software version 6.3) equipped with a Toshiba Teli CleverDragon 12 MP camera (and a lens with 50 mm focal length) was used. The analysis of the flat specimen was realized by a 2D setup at a grid size of 0.15 mm² at 16x16 pixels per facet and an overlap of 20 %. A linear strain calculation with a magnitude of 3 and a validity rate of 55% was applied. The region of interest was 25 mm (203 pixel) in length and 6 mm (35 pixel) in width. The system was calibrated with the help of a coded plate, the calibration deviation was 0.0023 pixel and the scale deviation 0.00 mm. To analyze static strain aging, the tensile tests were interrupted after defined plastic deformations of 20 % and 50 %. Samples were aged at room temperature for specific times (no aging, 3 days, 5 days). Aging was followed by tensile tests until failure. Due to the limited amount of material only one test per condition was carried out.

The aged samples of dimension 8 x 1 mm² were analyzed by small angle neutron scattering (SANS) at the beamline KWS-2 of the Jülich Centre for Neutron Science (JCNS) at the Heinz Maier-Leibnitz Zentrum (MLZ), Garching, Germany. With a neutron beam wavelength of $\lambda = 5 \text{ \AA}$, measurements were made at two detection distances, 1.74 m for the high Q region and 7.74 m for the low Q region. The collimation length was 8 m. The samples were measured in a 2.2 T transverse magnetic field to the beam axis achieved with an electromagnet. Evaluation was conducted using the software SASfit which is described elsewhere ^[37].

Results

Dynamic strain aging of the Fe-22Mn-1.3Al-0.3C was analyzed at room temperature at strain rates of $5 \times 10^{-6} \text{ s}^{-1}$, $2 \times 10^{-5} \text{ s}^{-1}$, $1 \times 10^{-4} \text{ s}^{-1}$, $1 \times 10^{-3} \text{ s}^{-1}$, $2.5 \times 10^{-3} \text{ s}^{-1}$ and $1 \times 10^{-2} \text{ s}^{-1}$

(**Figure 1a**). The according Yield Strength (YS), Ultimate Tensile Strength (UTS) and Total Elongation (TE) values are given in **Table 2**. The total elongation (TE) possesses a certain scattering and ranges from 56 % to 66 %. The YS is not affected by the change in strain rate. The UTS decreases with increasing strain rate from 961 MPa ($5 \times 10^{-5} \text{ s}^{-1}$) to 859 MPa ($1 \times 10^{-1} \text{ s}^{-1}$) by approximately 100 MPa. In this context, the decrease in tensile strength occurs linearly with a certain spread, if the strain rate is plotted logarithmically (**Figure 1b**). Thus, the strain rate sensitivity coefficient “m” of the extended Hollomon equation (Equation 1) is negative.

$$\sigma_t = k * \varphi^n * \dot{\varphi}^m \quad \text{Equation 1}$$

(σ_t is the true stress, **k** the Hollomon-constant, φ the logarithmic strain, **n** the strain hardening exponent and **m** the strain rate sensitivity coefficient.) The occurrence of serrated flow was recorded by means of digital image correlation and further analyzed. Strain localization was defined as a local strain rate increase, which is ≥ 5 times the global strain rate. The example shown in **Figure 1c** depicts the strain rate distribution at a strain rate of $2.5 \times 10^{-3} \text{ s}^{-1}$, where the onset of strain localization is identified at a critical strain (ϵ_{krit}) of approximately 41.5 % global engineering strain. The values of ϵ_{krit} for all strain rates are depicted in **Figure 1d**. At a strain rate of $1 \times 10^{-3} \text{ s}^{-1}$ the strain localization is observed at 40 % of strain, while occurring at higher global strain for higher and lower strain rates. A tendency regarding to the strength of strain localization from digital image correlation as a function of strain rate is not observed.

Table 2 Mechanical properties (YS, UTS and TE) at different strain rates.

Strain rate, s^{-1}	YS ($R_{P0.2}$), MPa	UTS, MPa	TE, %
5×10^{-6}	395	961	62.7
2×10^{-5}	389	922	63.9
1×10^{-4}	392	915	57.7
1×10^{-3}	392	902	66.2
2.5×10^{-3}	392	879	63.7
1×10^{-2}	389	859	55.7

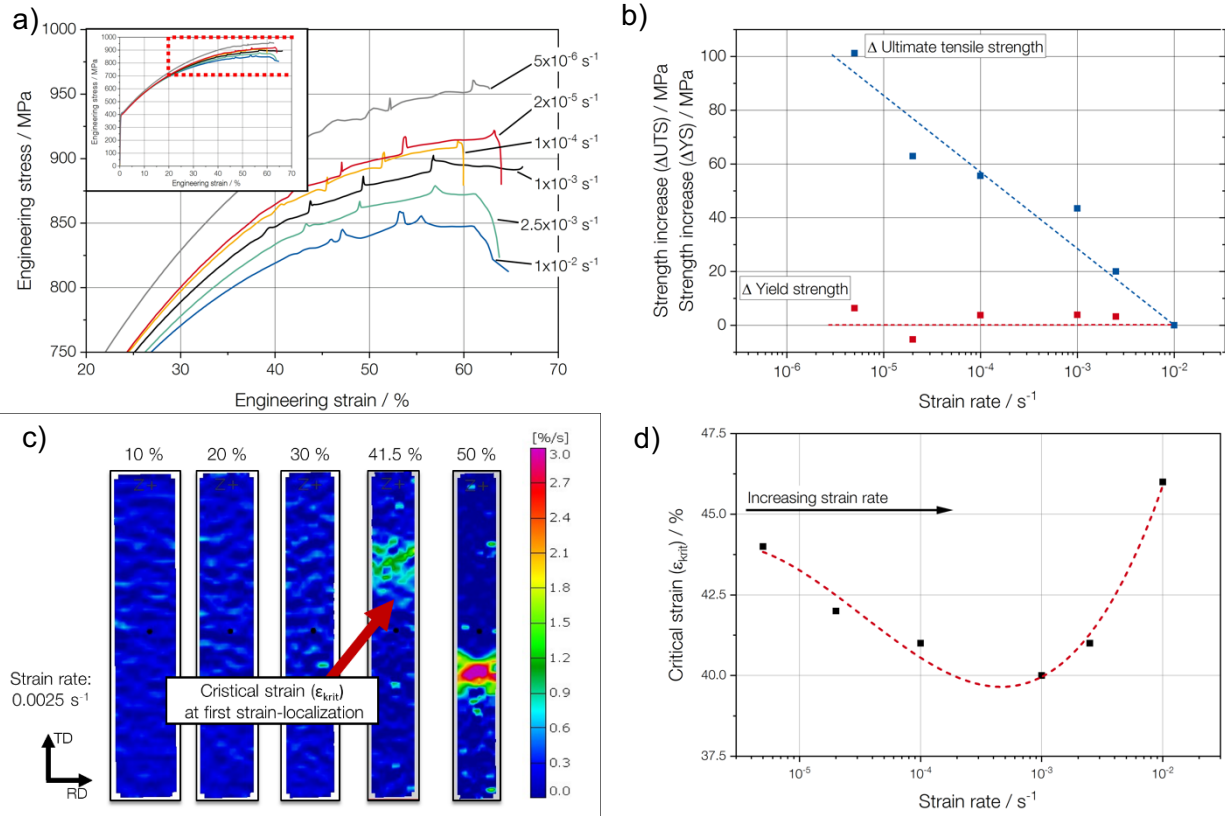


Figure 1 a) Stress strain curves at different strain rates with a magnification of the region showing dynamic strain aging; b) Strain rate related change of YS and UTS; c) Local longitudinal strain rate, from digital image correlation at global strain rate of $2.5 \times 10^{-3} \text{ s}^{-1}$; d) Critical strains (ϵ_{krit}) of the investigated strain rates.

To determine **static strain aging**, tensile tests at $2.5 \times 10^{-3} \text{ s}^{-1}$, (Figure 1 a) green line) were interrupted at engineering strains of 20 % and 50 %. After the material was pre-deformed, it was further tested immediately after unloading. For comparison and investigation of static strain aging, tensile tests were carried out 3 and 5 days after pre-deformation as well. YS [$R_{P0.2}$ (yield strength during continuous yielding) and R_e (yield strength during discontinuous yielding)] and UTS are listed in **Table 3**, the according stress strain curves are depicted in **Figure 2a**. Static strain aging after 20 % of elongation increases the YS by 19 MPa and 25 MPa after 3 days and 5 days respectively. A higher pre-deformation of 50 % had a greater effect on change of YS, 20 MPa and 30 MPa after 3 days and 5 days respectively. The stress increase (ΔYS) depicted in **Figure 2 b** is accommodated by a pronounced yielding, which was found in all samples after aging. The first Lüders band propagation was analyzed by digital image correlation as depicted in **Figure 2c**, the corresponding local strain-shift $\Delta \epsilon$ for all aging conditions are plotted in **Figure 2d**. 20 % pre-deformation this strain-shift ($\Delta \epsilon$) was low (0.1 %), while after 50 % of pre-deformation the shift was higher (2,6 %). Aging additionally effects this strain-shift, thus the highest $\Delta \epsilon$ was found after 50 % pre-deformation and 5 days aging (3.7 %). The work hardening is almost unaffected by aging and did not affect the TE after 20 % of pre-deformation. After 50 % pre-deformation, the TE decreases with increasing aging time (23.8 % \rightarrow 20.8 % \rightarrow 17.9 %).

Table 3 Mechanical properties at different times of room temperature aging.

Pre-deformation n, %	Aging Time, -	YS ($R_{P0.2}$), MPa	YS (R_e), MPa	UTS, MPa	TE, %	$\Delta\epsilon$, %
0 %	initial state	392	-	879	63.7	-
20 %	immediate	-	744	1028	49.3	0.1
20 %	3 days	-	763	1054	49.1	0.7
20 %	5 days	-	769	1064	48.6	1.3
50 %	immediate	-	1164	1251	23.8	2.6
50 %	3 days	-	1186	1269	20.8	3.2
50 %	5 days	-	1196	1271	17.9	2.6

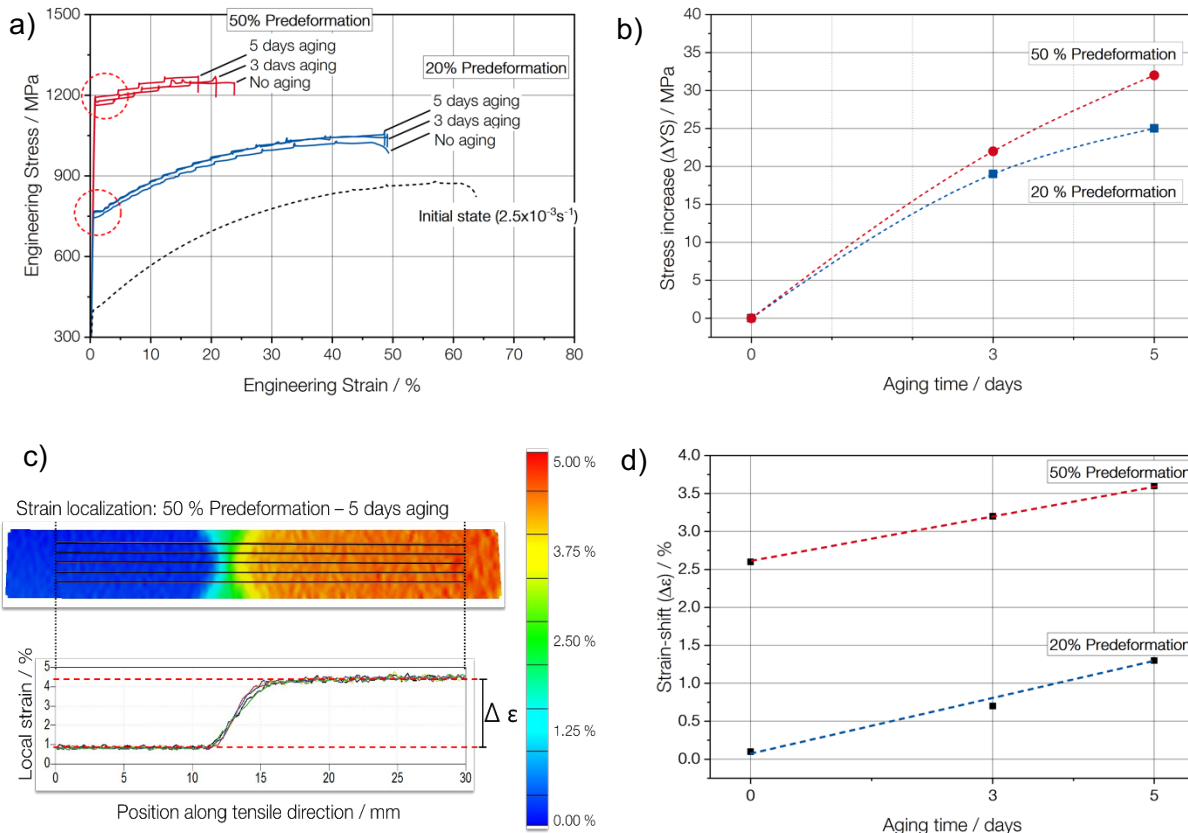


Figure 2 a) Stress-strain curves of the initial state and after 20 % and 50 % pre-deformation and aging; b) Stress increase due to aging after prestaining; c) Local distribution of strain along x-axis during pronounced yielding from digital image correlation after 50 % pre-deformation and 5 days of aging and depiction of strain increase $\Delta\epsilon$; d) Strain-shift during pronounced yielding from strain localization as shown in c).

The static strain aging was analyzed by small angle neutron scattering, which enabled to identify the size and number density of short-range ordered regions (**Figure 3**). Pre-deformation and aging led to a high number density of C-Mn ordered clusters in the order of 10^{18} . As shown in Figure 3 a), higher degree of pre-deformation, i.e. 50% pre-deformation, led to even higher number density and smaller size of the clusters. As shown in Figure 3 b), the number density of C-Mn ordered clusters increased with aging time. After 20 % of deformation aging resulted in a number density of 0.76×10^{18} and

1.37 $\times 10^{18}$ after 3 days and 5 days respectively. 50 % of pre-deformation increased number density after 3 days and 5 days to 1.64 $\times 10^{18}$ and 1.94 $\times 10^{18}$ respectively.

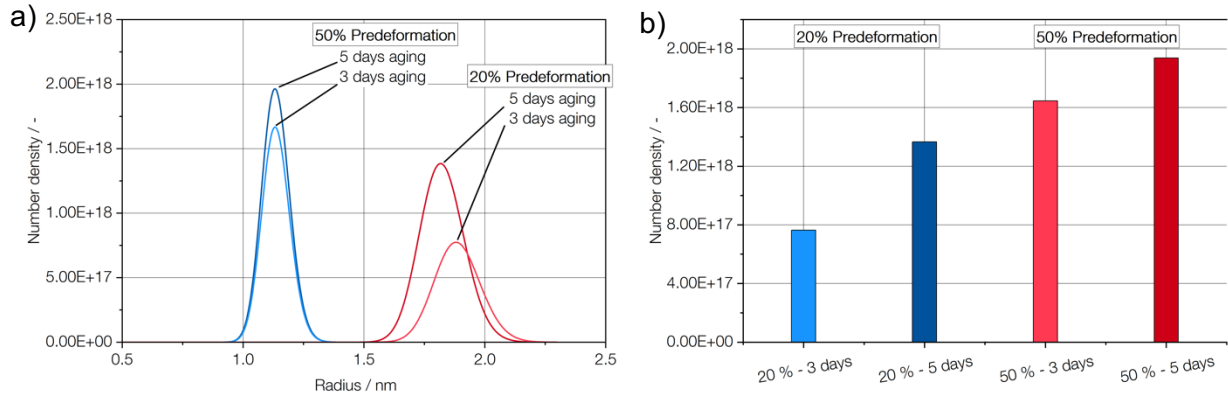


Figure 3 a) SANS results of the samples for different pre-deformation and aging times. b) Number density of the C-Mn ordered clusters at different deformation and aging states.

Discussion

The experimental results of the investigated austenitic high-manganese steel show a strong impact of aging on the mechanical properties (**Figure 1**, **Figure 2**) as well as on C-Mn ordering at nanoscale (**Figure 3**).

Our results show that shorter dynamic strain-aging, as from higher strain rate, resulted in a decrease in total strength, but does not affect the YS. The lack of effect on YS is likely due to the fact that plastic strain is an essential precondition for strain aging^[30]. The results show a change in total strength, which is as typical effect in high manganese steels and is accommodated by a negative strain rate sensitivity and a serrated flow^{[38][39][40][41]}. As some of the tensile samples were tested at strain rates above 10⁻³/s, we expect them to experience adiabatic heating as other authors have shown for austenitic steels^{[42][43]}. The higher temperature, which occurs after some plastic deformation, accelerates diffusive processes like aging. Although, we, as well as other authors, found that the increasing temperature leads to lower tensile strength, reduces strain hardening and retards the onset of serrated flow^{[39][44][45]}. However, at higher strain rates, several effects could occur simultaneously in addition to strain aging, making it hard to correlate our findings. For example, the tendency to planar slip is reduced, which reduces the formation of twins. The effects during dynamic strain aging make it difficult to assign the reasons for lower strength and later onset of serrated flow^{[46][47]}.

Static strain aging was investigated by interrupted tensile tests conducted at a constant strain rate of 2.5 $\times 10^{-3}$ s⁻¹. To analyze the processes of the nanostructure during static aging, the samples were examined with small angle neutron scattering additionally. The increase in YS, as known from other high-manganese steels, occurs due to strain aging^{[48][40]}. The increase in yield strength is repeatedly attributed to the hindrance of the dislocation movement or a combined effect of ordering and dislocation hindering^{[49][50][51]}. We found that the strength-increase intensifies with longer aging times and higher pre-

deformation (**Figure 2 b**). A higher pre-deformation comes along with a higher dislocation density, which as well increases the probability for the displacement of carbon atoms on tetrahedral interstitial sites during straining ^[52]. Subsequent aging leads to a reorientation, which is argued to influence dislocation movement and thus would lead to a strength increase ^[9]. This is a possible explanation, why pre-deformation and aging duration are related to strength increase.

In addition, we found a stronger localization of plastic strain with higher increase in yield strength. The plastic deformation localizes and a Lüders-band-like strain-shift occurs at the beginning of the plastic flow. Digital image correlation shows that the localization of plastic deformation is starting in the sample shoulders and moving along the parallel length of the sample. Reasons for localization probably have the same origin as localization during serrated flow and are still a matter of conjecture. Some authors state dislocation and twin substructures responsible for localization of strain ^{[53][54]}. Others point out that the interactions from C-Mn complexes are reasonable ^{[12][55]}. A combination of short-range ordering and twinning is stated by Sevsek et al. to be responsible for a serrated flow ^[49]. Even if none of the causes for localization of the strain is clear, our results show a clear relationship between the increase in stress, the intensity of the serrated flow and the formation of a short-range order.

Our results show that aging continues after deformation even at room temperature. Other studies used small angle neutron scattering as well but did not take aging at room temperature into account or accounted the increase in number density of C-Mn complexes solely to straining ^[56]. The influence of aging is accelerated by straining and the higher dislocation density. The increasing strength and the intensified strain-shift are accommodated by an increased number of C-Mn ordered clusters that arise during aging at room temperature. The analysis from small angle neutron scattering correlates a stronger pronounced yielding and a higher yield strength with a higher number of C-Mn complexes (**Figure 3**), which would suggest a causal relationship between strain aging and ordering. This is in agreement with some authors, stating ordering as origin of strain aging in high manganese steels ^{[49][33][12]}. Others, assume cluster formation is impossible, as they state the time needed to form C-Mn clusters is up to 10^{27} seconds ^[57]. A combined effect is stated to increase planar slip due to short range ordering and thus increase twinning, which would as well explain the stronger localization ^{[37][58][59]} as twinning promotes a serrated flow ^{[20][60][61]}. Other investigations even show that not only a higher pre-deformation intensifies strain aging, but show that an increase in temperature or a higher strain rate during pre-deformation further accelerate the static strain aging process ^{[48][40]}.

Even though our results show a correlation between C-Mn ordering and strength increase during static strain aging, this cannot be equally assumed for dynamic strain aging. This important aspect becomes apparent in the comparison of strain localization. During static strain aging, a clear increase in localization occurs after longer aging time. During dynamic strain aging, no strain rate dependent variance in the strength of the localization can be identified. Nevertheless, the findings show that dynamic as well as static strain aging increase the necessary stresses for plastic deformation as depicted in **Figure 4**. Static

strain aging increases the general strength level, dynamic strain aging affects the strain hardening during the tensile test.

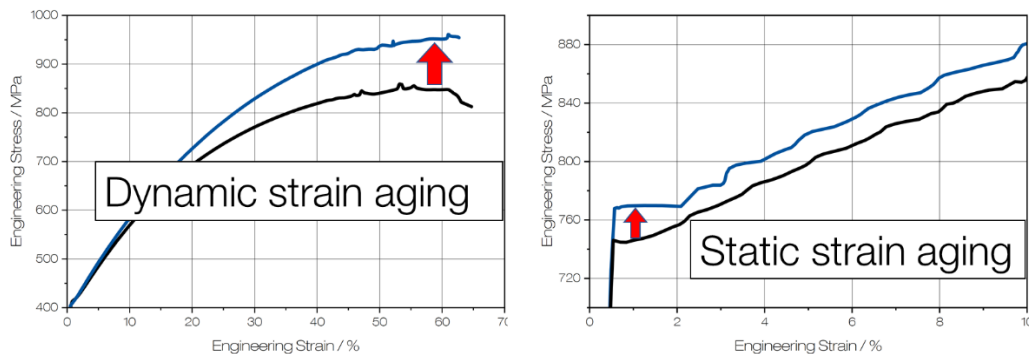


Figure 4: Impact of dynamic and static strain aging on mechanical properties

Conclusions

The static and dynamic strain aging of a high-manganese steel (Fe-22Mn-1.3Al-0.3C) has been investigated. The main conclusions are:

- A higher strain rate leads to an earlier onset of serrated flow during plastic deformation. However, this dependence is only valid until a strain rate of 10^{-3} is reached and adiabatic heating is expected.
- Static strain aging caused a pronounced yielding phenomenon in the investigated high manganese steel. Aging is influenced by the pre-deformation and the aging time. Both higher pre-deformation and longer aging time do not only increase the yield strength, but also increase the localization of strain during pronounced yielding.
- The observed aging phenomena are most probably related to C-Mn ordering. The microstructural regions affected by C-Mn ordering were quantified from small angle neutron scattering data.

Acknowledgements

The authors gratefully acknowledge the financial support of the DFG (Deutsche Forschungsgemeinschaft) within the collaborative research center SFB 761 “steel – ab initio”. In addition, we want to thank Nima Babaei, Marion Kreins and Daniela Wipp for their expertise and fruitful discussions throughout all aspects of our study.

References

- [1] G. Frommeyer, U. Brück, P. Neumann, *ISIJ Int.* **2003**, 43, 438–446.
- [2] M. Bambach, L. Conrads, M. Daamen, O. Güvenç, G. Hirt, *Materials & Design* **2016**, 110, 157–168.
- [3] S. Wesselmecking, M. Kreins, M. Dahmen, W. Bleck, *Materials & Design* **2022**, 213, 110357.
- [4] J.-H. Schmitt, T. Jung, *Comptes Rendus Physique* **2018**, 19, 641–656.
- [5] W. Bleck, *Int J Miner Metall Mater* **2021**, 28, 782–796.

- [6] S. Wesselmecking, M. Haupt, Y. Ma, W. Song, G. Hirt, W. Bleck, *Materials Science and Engineering: A* **2021**, 828, 142056.
- [7] G. Yang, J.-K. Kim, *Metals* **2021**, 11, 124.
- [8] W. Song, T. Ingendahl, W. Bleck, *ACTA METALL SIN* **2014**, 27, 546–556.
- [9] S.-I. Lee, S.-Y. Lee, J. Han, B. Hwang, *Materials Science and Engineering: A* **2019**, 742, 334–343.
- [10] Essoussi, H., Ettaqi, S., Essadiqi, E. H., *13ème Congrès de Mécanique* **2017**.
- [11] H. Kim, D.-W. Suh, N. J. Kim, *Science and technology of advanced materials* **2013**, 14, 14205.
- [12] S.-J. Lee, J. Kim, S. N. Kane, B. C. de Cooman, *Acta Materialia* **2011**, 59, 6809–6819.
- [13] L. Samek, E. de Moor, J. Penning, J. G. Speer, B. C. de Cooman, *Metall and Mat Trans A* **2008**, 39, 2542–2554.
- [14] S. Das, S. B. Singh, O. N. Mohanty, *Ironmaking & Steelmaking* **2011**, 38, 139–143.
- [15] H. K. D. H. Bhadeshia, *J Mater Sci* **2004**, 39, 3949–3955.
- [16] Jin-Kyung Kim, B.C. De Cooman, *steel research int.* **2009**, 2009, 493–498.
- [17] K. Renard, S. Ryelandt, P. J. Jacques, *Materials Science and Engineering: A* **2010**, 527, 2969–2977.
- [18] U. F. Kocks, R. E. Cook, R. A. Mulford, *Acta Metallurgica* **1985**, 33, 623–638.
- [19] R. A. Mulford, U. F. Kocks, *Acta Metallurgica* **1979**, 27, 1125–1134.
- [20] X. Bian, F. Yuan, X. Wu, *Materials Science and Engineering: A* **2017**, 696, 220–227.
- [21] P. Larour, A. Bäumer, K. Dahmen, W. Bleck, *steel research int.* **2013**, 84, 426–442.
- [22] J.-K. Kim, L. Chen, H.-S. Kim, S.-K. Kim, G. S. Kim, Y. Estrin, B. C. DeCooman, *Materials Technology* **2009**.
- [23] A. H. Cottrell, *The London, Edinburgh, and Dublin Philosophical Magazine and Journal of Science* **1953**, 44, 829–832.
- [24] J. S. Koehler, *Science (New York, N.Y.)* **1953**, 551–552.
- [25] A. V. Nazarov, A. A. Mikheev, *J. Phys.: Condens. Matter* **2008**, 20, 485203.
- [26] S.-J. Lee, D. K. Matlock, C. J. van Tyne, *ISIJ Int.* **2011**, 51, 1903–1911.
- [27] D. E. Jiang, E. A. Carter, *Phys. Rev. B* **2003**, 67, 214103.
- [28] H. K. D. H. Bhadeshia, R. W. K. Honeycombe, *Steels: Microstructure and properties*, Butterworth-Heinemann c/o Elsevier, Oxford **2007**.
- [29] P. Lan, J. Zhang, *Materials Science and Engineering: A* **2017**, 700, 250–258.
- [30] M. Koyama, T. Sawaguchi, K. Tsuzaki, *Tetsu-to-Hagane* **2018**, 104, 187–200.
- [31] Tanimoto H, *Newly Developed Method of Measurement for Conversion Electron Mossbauer Spectroscopy and its Applications in Material Sciences*, Osaka **1990**.
- [32] J. von Appen, R. Dronskowski, *steel research int.* **2011**, 82, 101–107.
- [33] J.-H. Kang, T. Ingendahl, J. von Appen, R. Dronskowski, W. Bleck, *Materials Science and Engineering: A* **2014**, 614, 122–128.
- [34] M. Grujicic, W. S. Owen, *Calphad* **1992**, 16, 291–299.

- [35] T. Hickel, S. Sandlöbes, R. Marceau, A. Dick, I. Bleskov, J. Neugebauer, D. Raabe, *Acta Materialia* **2014**, 75, 147–155.
- [36] R. Xie, S. Lu, W. Li, Y. Tian, L. Vitos, *Acta Materialia* **2020**, 191, 43–50.
- [37] W. Song, D. Bogdanovski, A. Yildiz, J. Houston, R. Dronskowski, W. Bleck, *Metals* **2018**, 8, 44.
- [38] J. B. Seol, J. G. Kim, S. H. Na, C. G. Park, H. S. Kim, *Acta Materialia* **2017**, 131, 187–196.
- [39] M. Madivala, W. Bleck, *JOM* **2019**, 71, 1291–1302.
- [40] M. Koyama, E. Akiyama, K. Tsuzaki, *ISIJ Int.* **2013**, 53, 1089–1096.
- [41] M. Koyama, E. Akiyama, K. Tsuzaki, *Scripta Materialia* **2012**, 66, 947–950.
- [42] N. I. Vázquez-Fernández, T. Nyyssönen, M. Isakov, M. Hokka, V.-T. Kuokkala, *Acta Materialia* **2019**, 176, 134–144.
- [43] N. I. Vazquez-Fernandez, G. C. Soares, J. L. Smith, J. D. Seidt, M. Isakov, A. Gilat, V. T. Kuokkala, M. Hokka, *J. dynamic behavior mater.* **2019**, 5, 221–229.
- [44] Y. F. Shen, N. Jia, R. Misra, L. Zuo, *Acta Materialia* **2016**, 103, 229–242.
- [45] R. Kapoor, S. Nemat-Nasser, *Mechanics of Materials* **1998**, 27, 1–12.
- [46] O. A. Zambrano, *J. Eng. Mater. Technol* **2016**, 138, 41010.
- [47] V. Gerold, H. P. Karnthaler, *Acta Metallurgica* **1989**, 37, 2177–2183.
- [48] S. Wesselmecking, W. Song, Y. Ma, T. Roesler, H. Hofmann, W. Bleck, *steel research int.* **2018**, 89, 1700515.
- [49] S. Sevsek, F. Brasche, C. Haase, W. Bleck, *Materials Science and Engineering: A* **2019**, 746, 434–442.
- [50] S. Sevsek, W. Bleck, *Metals* **2018**, 8, 34.
- [51] J.-H. Kang, T. Ingendahl, W. Bleck, *Materials & Design* **2015**, 340–349.
- [52] B. Hutchinson, N. Ridley, *Scripta Materialia* **2006**, 55, 299–302.
- [53] I. Gutierrez-Urrutia, D. Raabe, *Acta Materialia* **2011**, 59, 6449–6462.
- [54] S. D. Antolovich, R. W. Armstrong, *Progress in Materials Science* **2014**, 59, 1–160.
- [55] S. Hong, S. Y. Shin, J. Lee, D.-H. Ahn, H. S. Kim, S.-K. Kim, K.-G. Chin, S. Lee, *Metall and Mat Trans A* **2014**, 45, 633–646.
- [56] M. Kang, E. Shin, W. Woo, Y.-K. Lee, *Materials Characterization* **2014**, 96, 40–45.
- [57] S.-K. Oh, M. E. Kilic, J.-B. Seol, J.-S. Hong, A. Soon, Y.-K. Lee, *Acta Materialia* **2020**, 188, 366–375.
- [58] M. Koyama, T. Sawaguchi, K. Tsuzaki, *ISIJ International* **2015**, 55, 1754–1761.
- [59] V. Shterner, I. B. Timokhina, H. Beladi, *AMR* **2014**, 922, 676–681.
- [60] X.-J. Wang, X.-J. Sun, C. Song, H. Chen, S. Tong, W. Han, F. Pan, *Acta Metall. Sin. (Engl. Lett.)* **2019**, 32, 746–754.
- [61] T. A. Lebedkina, M. A. Lebyodkin, J.-P. Chateau, A. Jacques, S. Allain, *Materials Science and Engineering: A* **2009**, 519, 147–154.